Extracting polar anisotropy parameters from seismic data and well logs

Rongrong Lin[1] and Leon Thomsen[1,2]
[1] University of Houston,[2]Delta Geophysics

Summary

A new method is presented for extracting seismic polar anisotropy parameters, with the vertical resolution of the seismic wavelet, from prestack surface seismic data and vertical well logs. The method uses sonic V_{P0}, V_{S0} and ρ to construct an isotropic synthetic reflectivity gather, convolved with the (zero-phase) seismic wavelet, with no other propagation effects included. It uses a co-located surface CDP gather, in conjunction with this synthetic gather, to estimate the propagation effects. Then the arithmetic *difference* between the corrected seismic amplitudes and the isotropic synthetic amplitudes gives the jump in anisotropy parameters δ and ε at each major reflector in the logged interval. Integration of these differences, starting at a sandstone layer (with anisotropy assumed zero), yields a profile of the anisotropy itself. In a test case, this workflow yielded anisotropy parameters correlated with the gamma ray log. The anisotropic corrections were substantial.

Introduction

There is a need for a practical algorithm for estimating seismic anisotropy parameters with high spatial resolution. Surface seismic moveout yields estimates of anisotropy with low spatial resolution; sonic log data give no information at all on anisotropy. However, the workflow developed here offers the possibility that combining these data (and including log density and gamma ray data) can give estimates with the spatial resolution of the seismic wavelet. We describe the workflow below, in its logical stages. Most of the workflow is conventional, but we describe it in detail, to expose the assumptions, and to define the notation.

Given a borehole of sufficient depth, and a co-located CDP gather of surface seismic data, it is trivial to determine the anisotropy parameter δ, with low resolution in vertical time t_0, by comparison of the (seismic band) vertical velocity V_{P0seis} (*e.g.* from a VSP) with the moveout velocity V_{NMO} (from the CDP gather)(Thomsen, 1986, 2013):

$$V_{NMO}(t_0) = V_{P0Seis}(t_0)(1 + \delta(t_0)) \qquad (1)$$

However, if this calculation is performed with too-fine vertical resolution, it becomes numerically unstable. The present algorithm is intended to remedy this situation through the use of seismic and sonic amplitudes.

Log data

We begin with log data, for vertical velocities V_{P0}, V_{S0}, and density ρ, recorded and quality-controlled in conventional fashion, in a vertical borehole penetrating horizontal formations with assumed polar anisotropic symmetry. (If V_{S0} is not measured, it may be estimated, with corresponding reduction in confidence of the resulting computation.) The depths are converted to vertical travel times; at every logged point, and for a variety of assumed angles of incidence, a linearized isotropic reflection coefficient may be computed (*e.g.*, Rueger, 1997):

$$R_{iso}(t_0, \theta) \cong A_{iso} + B_{iso} \sin^2 \theta + \qquad (2)$$
$$C_{iso} \sin^2 \theta \tan^2 \theta$$

with

$$A_{iso}(t_0) = \frac{\Delta Z_{P0}}{2\bar{Z}_{P0}}$$

$$B_{iso}(t_0) = \frac{1}{2}\left[\frac{\Delta V_{P0}}{\bar{V}_{P0}} - \left(\frac{2\bar{V}_{S0}}{\bar{V}_{P0}} \right)^2 \frac{\Delta \mu_0}{\bar{\mu}_0} \right] \qquad (3)$$

$$C_{iso}(t_0) = \frac{1}{2}\left[\frac{\Delta V_{P0}}{\bar{V}_{P0}} \right]$$

where $Z_{P0} = \rho V_{P0}$ is vertical impedance, μ_0 is vertical shear modulus, Δ indicates a jump in properties between adjacent logged intervals (lower-upper), and the bar indicates an average across that interface.

From the associated seismic gather (discussed below), a wavelet is extracted, and converted to zero phase (here we assume that this wavelet $w(t_0)$ is independent of incidence angle). This is convolved with the reflectivity (1) to yield a (flattened) synthetic reflectivity gather:

$$s_{syn}(t_0, \theta) \equiv w(t_0) * R_{iso}(t_0, \theta)$$
$$= A_{syn}(t_0) + B_{syn}(t_0) \sin^2 \theta + \qquad (4)$$
$$C_{syn}(t_0) \sin^2 \theta \tan^2 \theta$$

where

$$A_{syn}(t_0) \equiv w(t_0) * A_{iso}(t_0)$$
$$B_{syn}(t_0) \equiv w(t_0) * B_{iso}(t_0) \qquad (5)$$
$$C_{syn}(t_0) \equiv w(t_0) * C_{iso}(t_0)$$

are computed quantities. Apart from propagation effects expressed by the seismic wavelet, there are no other propagation effects in s_{syn}.

Seismic data

We also require a co-located CDP gather of surface seismic data. It should be processed (pre-stack) to eliminate multiples and other noise, and converted to the angle domain. It should not be migrated, unless the migration algorithm is known to preserve relative amplitudes well. A super-gather may be used, to increase signal/noise. Ordinarily, the gather must be time-shifted and stretched/compressed in time to tie the synthetic gather (3), using conventional techniques.

The "convolutional model" of scalar seismic wave propagation describes this gather as:

$$s_{seis}(t, \theta) = C(t, \theta) * I(t, \theta) * P_\uparrow(t, \theta) *$$
$$r(t, \theta) * P_\downarrow(t, \theta) * w_0(t) * S_0(\theta) \tag{6}$$

which recounts the history of the wave, right-to-left. The operators shown above (discussed below) show an explicit dependence on of the incidence wavefront-angle θ at the eventual reflector, with an implicit dependence on the local ray-angle along the raypath. (See Thomsen (1986, 2013) for discussion of the difference between wavefront-angle and ray-angle in anisotropic media.) Since the operators depend upon frequency, and the frequency components combine linearly, the operators combine as convolutions.

The source-strength $S_0(\theta)$ includes the intrinsic source directivity, and also the interaction with the free surface (ghost, *etc*.). The time-signature of the source is given by the initial wavelet $w_0(t)$. The downward-propagating operator $P_\downarrow(\theta, t)$ includes the effects of geometric spreading, attenuation, transmission coefficients, "friendly multiples", focusing/defocusing, *etc*. The reflectivity series $r(\theta, t)$ is discussed further below.

The upward-propagating operator $P_\uparrow(\theta, t)$ includes the same effects as $P_\downarrow(\theta, t)$, but driven by the properties of the local medium on the upward leg of the ray. The instrumental operator $I(\theta, t)$ includes the instrumental impulse response, including coupling effects, as well as any interaction with the free surface. The computational operator $C(\theta, t)$ includes any processing that may have been done on the data.

It is clear that many of these operators cannot be determined, for field data. Nonetheless, we make progress,

as follows. First, we augment $C(\theta, t)$ to include flattening of the gather. Then, since convolution commutes, we re-arrange (6) as

$$s_{seis}(t_0, \theta) = [C(t_0, \theta) * I(t_0, \theta) * P_\uparrow(t_0, \theta) *$$
$$P_\downarrow(t_0, \theta) * S_0(\theta) * w_0(t_0)] * r(t_0, \theta) \tag{7}$$
$$= [P(t_0, \theta) * w(t_0)] * r(t_0, \theta)$$

where the propagation operator $P(t_0, \theta) * w(t_0)$ is compact notation for all the operators included in the square bracket above, and where $w(t_0)$ is the observed seismic wavelet.

The reflectivity series $r(t_0, \theta)$ is now assumed to be the linearized plane-wave reflectivity for polar anisotropic media:

$$r(t_0, \theta) \equiv R_{aniso}(t_0, \theta) \cong A_{aniso} + B_{aniso} \sin^2 \theta$$
$$+ C_{aniso} \sin^2 \theta \tan^2 \theta \tag{8}$$

wit

$$A_{anis}(t_0) = A_{iso}(t_0)$$
$$B_{aniso}(t_0) = B_{iso}(t_0) + \Delta\delta(t_0)/2 \tag{9}$$
$$C_{aniso}(t_0) = C_{iso}(t_0) + \Delta\varepsilon(t_0)/2$$

In analogy with (4, 8), we parameterize the angular variation of the seismic data (7) with

$$s_{seis}(t_0, \theta) = [A_{seis}(t_0) + B_{seis}(t_0) \sin^2 \theta +$$
$$C_{seis}(t_0) \sin^2 \theta \tan^2 \theta] \tag{10}$$

Combining log and seismic data

At this point, the analysis may proceed either in terms of band-limited ("wiggle") traces, or as discrete ("sparse-spike") reflectivity impulses. Here, we choose the latter approach. We write

$$\hat{A}_{seis}(t_0) \equiv w * \dddot{A}_{seis}(t_0)$$
$$\hat{B}_{seis}(t_0) \equiv w * \dddot{B}_{seis}(t_0) \tag{11}$$
$$\hat{C}_{seis}(t_0) \equiv w * \dddot{C}_{seis}(t_0)$$

The impulse functions $\dddot{A}_{seis}(t_0), \dddot{B}_{seis}(t_0), \dddot{C}_{seis}(t_0)$ may be found manually or by sparse-spike inversion; they must occur only at times t_0 for which a correlative event occurs in the synthetic gather (4). These spikes represent the central peaks (or troughs) of each major event in the zero-

phase data, over the logged interval, as a function of angle θ, and $\ddot{A}_{seis}(t_0), \ddot{B}_{seis}(t_0), \ddot{C}_{seis}(t_0)$ are found as best fits to these data, of the Aki-Richards form

$$[\dddot{A}_{seis} + \ddot{B}_{seis}\sin^2\theta + \ddot{C}_{seis}\sin^2\theta\tan^2\theta] \quad (12)$$

Standard statistical measures are applied to test the confidence with which the low-order terms $\ddot{B}_{seis}(t_0), \ddot{C}_{seis}(t_0)$ are determined; if the seismic data is too noisy, then either or both is poorly determined, and the analysis of such terms should not proceed.

With this subset of events, the resulting reduced seismic gather is written as

$$\hat{s}_{seis}(t_0,\theta) = \sum_{t_0}[\hat{A}_{seis}(t_0) + \hat{B}_{seis}(t_0)\sin^2\theta +$$
$$\hat{C}_{seis}(t_0)\sin^2\theta\tan^2\theta] \quad (13)$$

where only the selected events are included in the sum, and $\hat{A}_{seis}(t_0), \hat{B}_{seis}(t_0), \hat{C}_{seis}(t_0)$ are defined in (11).

Here, in equations (8-13) (underline in equation (4)), the angles θ are computed from the *offsets* in the original data, and the estimated velocity function in the overburden. Hence, they may be in error, from an incorrect velocity profile. In addition, the angles computed from offsets in the conventional manner are ray-angles, and must be converted to wavefront angles θ, using the anisotropy profile in the overburden, *c.f.* equation (1) (Thomsen, 1986, 2013). Errors made in this computation translate directly into corresponding errors in the coefficients (12). However, such errors will be compensated for in the workflow below.

In analogy with the analysis of the seismic data (13), we select a series of reflectivity spikes (either by manual picking, or by sparse spike inversion) to represent major events in the synthetic data (4). We call those spikes $\dddot{A}_{syn}(t_0), \ddot{B}_{syn}(t_0), \ddot{C}_{syn}(t_0)$, found from the synthetic data (4) as best-fits of the Aki-Richards form,. Convolving these with the zero-phase seismic wavelet:

$$\hat{A}_{syn}(t_0) \equiv w * \dddot{A}_{syn}(t_0)$$
$$\hat{B}_{syn}(t_0) \equiv w * \ddot{B}_{syn}(t_0) \quad (14)$$
$$\hat{C}_{syn}(t_0) \equiv w * \ddot{C}_{syn}(t_0)$$

we form the reduced synthetic data as

$$\hat{s}_{syn}(t_0,\theta) = \sum_{t_0}[\hat{A}_{syn}(t_0) + \hat{B}_{syn}(t_0)\sin^2\theta +$$
$$\hat{C}_{syn}(t_0)\sin^2\theta\tan^2\theta] \quad (15)$$

(This treatment of the synthetic data is necessary, to preserve the analogy with the reduced seismic data (13).)

The seismic gather (13) has the same form as the synthetic gather (14), except for the inclusion in the former of the (unknown) propagation operator $P(t_0,\theta)$. Included in P are the instrumental and computational operators (I and C), which impose large gain factors on the data. The seismic data (13) usually have an absolute maximum value $< 10^4$ (we may call these "seismic units", with unknown physical dimensions), whereas the synthetic data (15) usually have an absolute maximum value < 1 (nondimensional "reflectivity units"). Without loss of generality, we may augment the computational operator C with a multiplicative divisor, to make the amplitudes (on synthetic and seismic) *comparable*, in order to display them on the same plot. We choose to multiply all the seismic amplitudes by the factor

$$N_0 \equiv \left\langle\left|\ddot{A}_{syn}\right|\right\rangle / \left\langle\left|\ddot{A}_{seis}\right|\right\rangle \quad (16)$$

(*c.f.* equations (11, 14) where the angle brackets represent an arithmetic average over the selected events in the logged interval, and the bars represent absolute values.

Normally, these adjusted-seismic and synthetic amplitudes will show significant differences from each other, since the seismic data contain the effects of both propagation and of anisotropy, whereas the synthetic data do not.

We form the normalizing functions

$$N_A(t_0) \equiv \dddot{A}_{syn}(t_0) / N_0 \dddot{A}_{seis}(t_0)$$
$$N_B(t_0) \equiv \ddot{B}_{syn}(t_0) / N_0 \ddot{B}_{seis}(t_0) \quad (17)$$
$$N_C(t_0) \equiv \ddot{C}_{syn}(t_0) / N_0 \ddot{C}_{seis}(t_0)$$

which are defined only at the selected values of t_0. If we were to multiply the seismic data $\dddot{A}_{aeis}(t_0), \ddot{B}_{aeis}(t_0), \ddot{C}_{aeis}(t_0)$ by these normalizing functions, this would simply force the seismic data to match the isotropic synthetic data.

Instead, we recognize that $N_A(t_0), N_B(t_0), N_C(t_0)$ are time-series, each with a Fourier spectrum. We examine the propagation operator $P(t_0,\theta)$ in (7), and observe that all

of the propagation effects, included in it, accumulate <u>progressively</u> as the wave propagates, hence they contribute to the <u>low</u>-frequency parts of these spectra. By contrast, the reflectivity operator $r(t_0,\theta)$ in (7,8) fluctuates <u>rapidly</u> in time, contributing only to the <u>high</u>-frequency parts of these spectra.

Hence, we low-cut filter the normalization functions, obtaining $N_{Alow}(t_0), N_{Blow}(t_0), N_{Clow}(t_0)$ (the design of the low-pass operation may require some interpretive judgment). Then, we <u>multiply</u> the seismic amplitudes $\ddot{A}_{aeis}(t_0), \ddot{B}_{aeis}(t_0), \ddot{C}_{aeis}(t_0)$ by these <u>low-cut</u> normalization functions; the resulting amplitudes should be identical to the isotropic amplitudes $\ddot{A}_{syn}(t_0), \ddot{B}_{syn}(t_0), \ddot{C}_{syn}(t_0)$ except for the <u>additive</u> effects of anisotropic reflectivity (*c.f.* (8):

$$N_{Alow}(t_0)\ddot{A}_{seis}(t_0) - \ddot{A}_{syn}(t_0) = 0 \qquad (18a)$$

$$N_{Blow}(t_0)\ddot{B}_{seis}(t_0) - \ddot{B}_{syn}(t_0) = \Delta\delta/2 \qquad (18b)$$

$$N_{Clow}(t_0)\ddot{C}_{seis}(t_0) - \ddot{C}_{syn}(t_0) = \Delta\varepsilon/2 \qquad (18c)$$

If equation (18a) is not fulfilled by the data, this is not consistent with the present assumptions, and not interpretable in terms of anisotropy. There are two possible explanations:

  a) The computational operator **C** has not removed all multiples, and/or
  b) The reflectivity operator *r(t₀, θ)* is not a plane-wave / planar reflector operator, such as is given in equation (8).

In the first case, the multiples should be removed, *e.g.* by an *f-k* filtering operation, and the analysis repeated. The second case is more fundamental, as it requires a deep re-assessment of the reflection process. In the following, we assume that equation (18a) is respected by the data, with sufficient accuracy.

To convert the computed jumps $\Delta\delta, \Delta\varepsilon$ in (18bc) to absolute values δ, ε , it is only necessary to identify, from the gamma-ray log, an interval of sandstone, and to assign $\delta, \varepsilon = 0$ to that layer. Then the parameters in the other layers may be found directly, *e.g.:*

$$\delta_2 = \delta_1 + \Delta\delta \qquad (19)$$

It often happens that the amplitudes $\ddot{C}_{aeis}(t_0)$ are poorly determined, since it is common for this curvature parameter to be strongly affected by seismic noise. If the parameters

$\varepsilon(t_0)$ determined by this workflow are not reasonable (e.g. if they are < 0 or > 0.2, this is the most likely cause.

**Example**

This workflow was applied (Lin, 2013) to the "Colony" dataset supplied with Hampson-Russell software. The figure below shows the amplitudes $\ddot{B}_{syn}(t_0)$ (15), $N_0\ddot{B}_{seis}(t_0)$ (12, 16), and $N_{Blow}\ddot{B}_{seis}(t_0)$ (18), for the six major events in the logged interval. (The determination of the seismic parameter $\ddot{C}_{seis}(t_0)$ was not statistically reliable.) As expected, the anisotropic contributions $\left(N_{Blow}\ddot{B}_{seis} - \ddot{B}_{svn}\right)$ are significant.
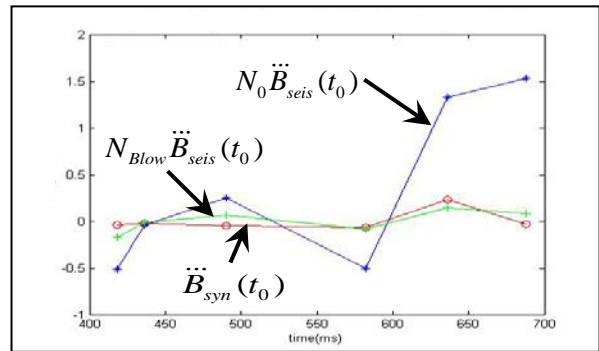
The figure below shows the resulting values for the anisotropy parameter δ, compared with the gamma-ray log, plotted at the same scale; the correlation is good.
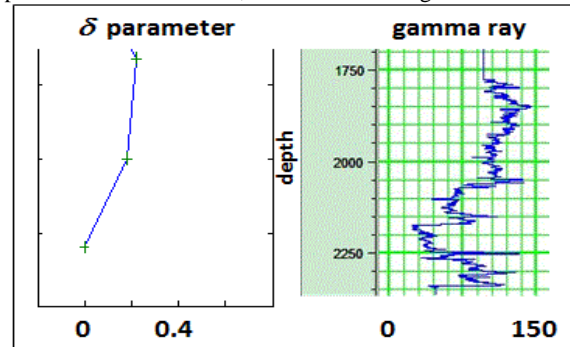
Conclusions

This workflow appears, on the basis of initial tests, to yield values of the anisotropy parameter δ, which have the spatial resolution of the seismic wavelet, which correlate well with shale lithology (as measured by the gamma-ray log), and which are substantial in magnitude.

EDITED REFERENCES

Note: This reference list is a copy-edited version of the reference list submitted by the author. Reference lists for the 2013 SEG Technical Program Expanded Abstracts have been copy edited so that references provided with the online metadata for each paper will achieve a high degree of linking to cited sources that appear on the Web.

REFERENCES

Lin, R., 2013, Extracting polar anisotropy parameters from seismic data and well logs: M. S. thesis, University of Houston.

Nye, J. F., 1985, Physical properties of crystals: Their representation by tensors and matrices: Oxford University Press.

Rueger, A., 1998, Variation of P-wave reflectivity with offset and azimuth in anisotropic media: Geophysics, **63**, 935–947, http://dx.doi.org/10.1190/1.1444405.

Thomsen, L., 1986, Weak elastic anisotropy: Geophysics, **51**, 1954–1966, http://dx.doi.org/10.1190/1.1442051.

Thomsen, L., 2010, Weakly anisotropic elastic compliance: 72nd Annual International conference and Exhibition, EAGE, Extended Abstracts, 7.

Thomsen, L., 2013, Understanding seismic anisotropy in exploration and exploitation, 2nd ed.: SEG.